

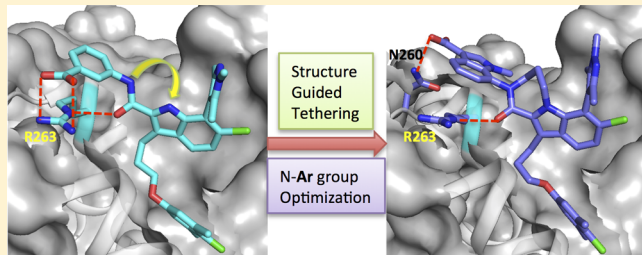
## Optimization of Potent and Selective Tricyclic Indole Diazepinone Myeloid Cell Leukemia-1 Inhibitors Using Structure-Based Design

Subrata Shaw,<sup>†</sup> Zhiguo Bian,<sup>†,§</sup> Bin Zhao, James C. Tarr, Nagarathanam Veerasamy, Kyu Ok Jeon, Johannes Belmar, Allison L. Arnold, Stuart A. Fogarty, Evan Perry, John L. Sensintaffar, DeMarco V. Camper, Olivia W. Rossanese,<sup>†</sup> Taekyu Lee, Edward T. Olejniczak, and Stephen W. Fesik\*,<sup>¶</sup>

Department of Biochemistry, Vanderbilt University School of Medicine, 2215 Garland Avenue, 607 Light Hall, Nashville, Tennessee 37232-0146, United States

### Supporting Information

**ABSTRACT:** Myeloid cell leukemia 1 (Mcl-1), an antiapoptotic member of the Bcl-2 family of proteins, has emerged as an attractive target for cancer therapy. Mcl-1 upregulation is often found in many human cancers and is associated with high tumor grade, poor survival, and resistance to chemotherapy. Here, we describe a series of potent and selective tricyclic indole diazepinone Mcl-1 inhibitors that were discovered and further optimized using structure-based design. These compounds exhibit picomolar binding affinity and mechanism-based cellular efficacy, including growth inhibition and caspase induction in Mcl-1-sensitive cells. Thus, they represent useful compounds to study the implication of Mcl-1 inhibition in cancer and serve as potentially useful starting points toward the discovery of anti-Mcl-1 therapeutics.



### INTRODUCTION

The Bcl-2 (B cell lymphoma 2) family of proteins, comprised of antiapoptotic, proapoptotic, and executioner proteins, are critical regulators of apoptosis/programmed cell death.<sup>1–4</sup> The antiapoptotic proteins in the Bcl-2 family (Bcl-2, Bcl-xL, Bcl-w, Bcl-A1, and Mcl-1 (myeloid cell leukemia 1)) bind to and sequester both the proapoptotic (Bim, Bid, Bad, PUMA, NOXA) and executioner (Bak, Bax) members of the Bcl-2 family, thereby preventing Bak and Bax oligomerization.<sup>1,2</sup> This results in the permeabilization of the mitochondrial membrane, cytochrome *c* release, and the commitment of the cell to undergo apoptosis.<sup>5</sup> Thus, upregulation of one or more of the antiapoptotic Bcl-2 family proteins may allow cancer cells to evade apoptosis, fulfilling one of the hallmarks of cancer.<sup>1,6,7</sup> Upregulation of the Mcl-1 protein and/or amplification of the *MCL1* gene have been linked to a variety of human cancers,<sup>8,9</sup> including lung, breast, pancreatic, cervical, and ovarian cancers as well as leukemia and lymphoma.<sup>10–17</sup> Mcl-1 upregulation is directly responsible for the emerging resistance of various FDA-approved anticancer therapies, including vincristine, taxol, gemcitabine, and cisplatin.<sup>18,19</sup> Moreover, downregulation of Mcl-1 by RNAi decreases tumorigenicity in mouse xenograft models.<sup>19</sup> These observations suggest that the inhibition of Mcl-1 may provide a promising strategy to induce apoptosis in cancer cells by blocking a critical survival mechanism.

Targeting proteins of the Bcl-2 family has proven to be challenging due to the tight binding between members of the family through a large protein–protein interface.<sup>21</sup> All members of the Bcl-2 family possess a conserved BH3 domain consisting of an amphipathic  $\alpha$ -helix containing four key hydrophobic

residues (H1–H4: L210, L213, V216, V220 in Mcl-1), which bind to four corresponding hydrophobic pockets (P1–P4) on antiapoptotic Bcl-2 family proteins.<sup>7,22–24</sup> Small molecules capable of disrupting this binding interaction are expected to release proapoptotic Bcl-2 family proteins and restore Bak and Bax function in the apoptotic pathway. The concept of targeting antiapoptotic Bcl-2 family proteins has been validated with the Bcl-2-selective inhibitor Venetoclax (ABT-199) that has recently received FDA approval for the treatment of chronic lymphocytic leukemia (CLL).<sup>25–27</sup> ABT-263 (Navitoclax), a Bcl-xL, Bcl-w, and Bcl-2 inhibitor, has also achieved clinical efficacy but exhibits toxicity arising from thrombocytopenia.<sup>28–30</sup> Both of these compounds exhibit minimal affinity for Mcl-1, and the major cause of resistance to treatment with these inhibitors is the upregulation of Mcl-1. However, like the other members of the family, the discovery of potent Mcl-1 inhibitors has been difficult to achieve. In addition to the difficulties in targeting protein–protein interactions for the Bcl-2 family proteins is the need to achieve extremely potent binding affinities (often subnanomolar) before realizing cellular efficacy.<sup>31</sup> This is most likely due to the potent binding affinity of full length pro- and antiapoptotic family members at the mitochondrial membrane surface.

Despite these difficulties, several groups (Servier-Vernalis in collaboration with Novartis,<sup>32–36</sup> Amgen,<sup>37</sup> and Astra-Zeneca<sup>38</sup>) have reported the discovery of Mcl-1 inhibitors that have recently entered clinical development. These compounds

Received: November 9, 2017

Published: January 11, 2018



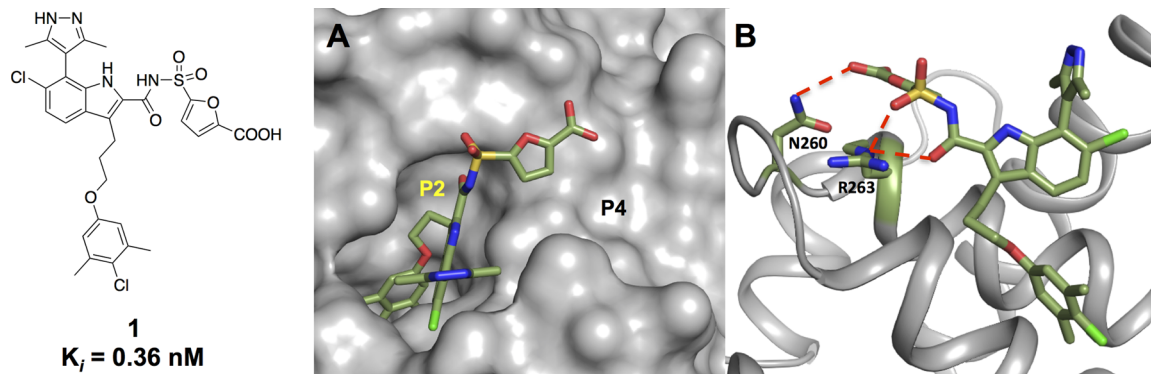


**Figure 1.** Compound 1 (A) X-ray cocrystal structure of compound 1 bound to Mcl-1 (SFDR). (B) Polar interactions between acylsulfonamide and terminal COOH with R263 and N260, respectively.

exhibited robust in vivo efficacy and achieved tumor regression in mouse xenograft models. In addition, they appeared to be well tolerated at efficacious doses. These data demonstrate that Mcl-1 can be druggable by a small molecule inhibitor and suggest that a safe therapeutic window may be achievable.

We have previously reported on the discovery of potent Mcl-1 inhibitors<sup>39–41</sup> from an initial 2-indole carboxylic acid lead<sup>39</sup> to a series of extended 2-indole-acylsulfonamides that occupy a wider binding interface within the binding groove on Mcl-1.<sup>41</sup> Using structure-based design, a highly potent and selective Mcl-1 inhibitor (compound 1) was discovered. Compound 1 exhibits a  $K_i$  of 0.36 nM for Mcl-1 and >10000-fold selectivity over Bcl-xL.<sup>40</sup> An X-ray cocrystal structure of compound 1 bound to Mcl-1 reveals that the indole core unit occupies the P2 pocket of Mcl-1, where the acylsulfonamide moiety engages a charge–charge interaction with R263. In addition, the terminal carboxylic acid on the furan is positioned within H-bonding distance to the amide NH of N260, forming an additional polar contact to the protein (Figure 1).<sup>41</sup> However, compound 1 failed to show convincing antiproliferative activity in Mcl-1-sensitive cells despite its sub-nM affinity. This is probably due to its poor pharmaceutical properties. Indeed, compound 1 does not show any measurable permeability in the parallel artificial membrane permeability assay (PAMPA) and exhibits significantly reduced Mcl-1 affinity in the presence of 1% fetal bovine serum (FBS) in a biochemical assay due to high protein binding resulting from the presence of the two acidic functional groups.

Here, we describe the discovery and optimization of small molecule Mcl-1 inhibitors that contain a novel tricyclic indole diazepinone core unit. Early compounds (29 and 30) in the series exhibited promising biological activities.<sup>42</sup> In this paper, we describe more advanced Mcl-1 inhibitors within the series with improved potency and pharmaceutical properties. These compounds were obtained using X-ray structure-guided modifications. These new Mcl-1 inhibitors exhibit picomolar binding affinities and on-target mechanism-based antiproliferative activity in Mcl-1-sensitive cells.

## RESULTS

**Feasibility Assessment for Replacing the Acylsulfonamide with an Amide.** To improve the druglike properties of 1 while maintaining the high on-target potency of the compound, we explored the possibility of replacing the acidic acylsulfonamide unit with a neutral amide linkage as a synthetic handle recognizing that this strategy might eliminate the critical

charge–charge interaction with R263 (Figure 1). To partially mitigate this potential loss of affinity, the terminal carboxylic acid with varying linker units was conserved to mimic the binding interaction with N260 that was observed with compound 1. The strategy was further supported by our initial NMR-based fragment screening results in which we identified a cluster of heterobicycles containing an extended carboxylic acid through a flexible linker unit.

As a model study, compounds 3–6 were prepared to assess the feasibility of the new design concept by comparing their Mcl-1 binding affinities to methyl acylsulfonamide 2 as a reference compound (Table 1). The glycine methyl ester

**Table 1.** Mcl-1  $K_i$ 's of Model 2-Indole Amides

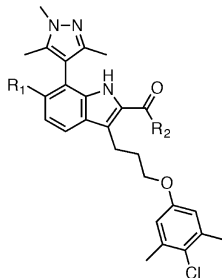
Comp.	X	$K_i$ (nM)
2	<chem>CS(=O)(=O)N</chem>	$655 \pm 400$
3	<chem>NC(=O)O</chem>	$3200 \pm 2600$
4	<chem>NC(=O)O</chem>	$620 \pm 110$
5	<chem>NC(=O)O</chem>	$570 \pm 110$
6	<chem>NC1=CSC=C1C(=O)O</chem>	$69 \pm 16$

coupled amide 3 showed a 5-fold decrease in affinity compared to that of 2, reaffirming the importance of an acidic group at the site. This loss of potency was quickly recovered by reintroducing the carboxylic acid functionality in compounds 4 and 5, which exhibit  $K_i$ 's equal to acylsulfonamide 2. The biggest improvement in affinity was observed in compound 6 by incorporating the 2-furyl carboxylic acid moiety of compound 1 with a 10- and 47-fold enhancement from compounds 2 and 3, respectively. These results demonstrate the effectiveness of this strategy.

**Mcl-1 Affinity Optimization of 2-Indole Amides.** The binding affinities of the 2-indole amide series were further

optimized by incorporating substitutions that improved affinity based on our earlier SAR.<sup>39–41</sup> For example, the incorporation of 6-Cl and 7-aryl groups resulted in an affinity enhancement similar to that observed for the 2-indole acids<sup>39,40</sup> and acylsulfonamides.<sup>41</sup> Consistent with the earlier SAR, installation of the 7-(1,3,5-trimethyl-1*H*-pyrazol-4-yl) group in compound 7 caused a 4-fold increase in potency compared to that of compound 6, and the 6-Cl analogue (9) of compound 8 also exhibited a 4-fold higher affinity to Mcl-1. These results suggest that the core unit SAR trend of the 2-indole amide is similar to the previously reported 2-indole acid and acylsulfonamide series, and favorable modifications found in these chemotypes could be employed to facilitate the optimization process. We next explored 6-membered aromatic congeners in place of the furan with varying linker length and positions of the carboxylic acid (Table 2). The location of the carboxylic acid in 7 suggests

**Table 2.** Binding Affinities of 2-Indole Amides Containing Extended Aromatic Acids



Comp.	R <sub>1</sub>	R <sub>2</sub>	K <sub>i</sub> (nM)		Permeability PAMPA (10 <sup>-6</sup> cm/s)
			Mcl-1	1% FBS <sup>a</sup>	
7	H		19 ± 4.8	174 ± 125	
8	H		72 ± 65	>200	
9	Cl		20 ± 5.3	102 ± 55	<7.6
10	H		41 ± 9.3	165 ± 65	<1.2
11	H		21 ± 9.0	>200	
12	Cl		23 ± 4.0	108 ± 33	<3.3
13	Cl		17 ± 2.0	139 ± 51	<1.0
14	Cl		96 ± 27	>200	<1.6
15	Cl		12 ± 4.0	>200	<3.3
16	Cl		31 ± 1.5	>200	2.3
17	Cl		22 ± 7.1	>200	1.2
18	Cl		29 ± 4.6	>200	<2.3

<sup>a</sup>Mcl-1 K<sub>i</sub> in the presence of 1% fetal bovine serum.

both meta and para arrangements of the moiety could be accommodated in a 6-membered aromatic ring. Indeed, *para*-benzyl congener 11 shows comparable potency to that of furan 7 and 3-fold higher affinity than that of *meta*-analogue 8.

Compounds 12–18 were synthesized by coupling aromatic amines to the optimized 2-indole acid core, and their binding affinities to Mcl-1 were measured (Table 2). Surprisingly, they retain high binding affinities to Mcl-1 with the exception of compound 14. We also found that *meta*- and *para*-carboxylic acids 12 and 17, respectively, are favorable substitutions unlike the analogous homologues 8 and 11. These observations suggest that the aromatic acid unit in compounds 7–11 could be involved in quite different binding interactions with Mcl-1 compared to those of their shorter homologues 12–18. In

addition, both 5- and 6-membered pharmaceutically desirable heterocycles could replace the hydrophobic phenyl group to modulate druglike properties without losing potency. Despite enhanced binding affinities, all examples in Table 2 continued to show a significant shift in K<sub>i</sub> by the addition of 1% FBS and minimal permeability in PAMPA. Therefore, additional modifications were necessary to significantly enhance both the potency and pharmaceutical properties of the series.

**X-ray Cocrystal Structure of Indole Amide 12 Bound to Mcl-1.** The X-ray cocrystal structure of 12 complexed with Mcl-1 was obtained in an attempt to understand the binding interactions that favor complex formation (Figure 2). Interestingly, the asymmetric unit of the crystal structure contains four copies of the complexes with two equally populated 3-benzoic acid conformations of amide 12 resulting in two different locations of the carboxylate moiety. The indole core unit and the extended phenyl amide portion of both conformers of 12 adopt nearly superimposable poses in the hydrophobic P2 pocket. The carbonyl of the amide and 6-Cl maintain favorable electrostatic interactions with R263 and the backbone carbonyl of A227, respectively, similar to that observed in previously reported structures.<sup>39,42</sup> In addition, the phenyl moiety linked to the amide group sits atop the positively charged guanidinium group of R263 (R263 shelf) to form a stabilizing cation–π interaction. Intriguingly, the benzoate moiety of the two observed conformers utilizes different polar contacts in the shelf region to form a stable complex with Mcl-1. The carboxylate of the first pose (cyan) (Figure 2A, B) is positioned above the guanidinium of R263 to elicit a charge–charge interaction, whereas a H-bond with the side chain NH of N260 is observed in the second pose (yellow Figure 2B). In both cases, these newly discovered binding interactions involving the 3-benzoate group are consistent with the enhanced binding affinity. An overlay of the crystal structures of cocomplexes 1 and 12 (Figure 2C) reveal that the benzoate of 12 is located at a different part of the shelf relative to the furanoate of 1, rationalizing the distinctive SAR trends observed between the benzyl (7–11) and phenyl (12–18) amide series of Mcl-1 inhibitors. The cocomplex structures also reveal that the extended aromatic acid portion of this series occupies only a fraction of the R263 shelf region and suggest further opportunities for optimizing potency in this site.

**Formation of Tricyclic Indole-Diazepinone.** The Mcl-1 bound conformation of amide 12 (Figure 2D) shows that the indole amide portion of the molecule is nearly coplanar and that the two NHs adopt an ideal geometry for tethering to form a ring structure. Accordingly, the two nitrogens of the 2-indole amide moiety were linked together to give the tricyclic indole-diazepinones 19–27. Their biological activities are summarized in Table 3. In general, the tricyclic series of Mcl-1 inhibitors exhibited significantly enhanced Mcl-1 affinities when compared with their direct open-chain amide analogues. By rigidifying the bound conformation, a 5-fold increase in binding was observed for benzylic acid 20 with or without 1% FBS from amide 9. In addition, by removing the two H-bond donors, compound 20 becomes highly permeable in PAMPA. The tethering strategy is even more impactful for the benzoic acid analogs 23–27, in which >10-fold enhancement in Mcl-1 affinity was observed compared to their open-chain counterparts. These compounds exhibited low nM K<sub>i</sub>'s, and compounds 23, 24, and 26 displayed minimal shifts in binding affinity by the addition of 1% FBS. It is also noteworthy that equally potent regioisomers 24 and 25 show remarkably

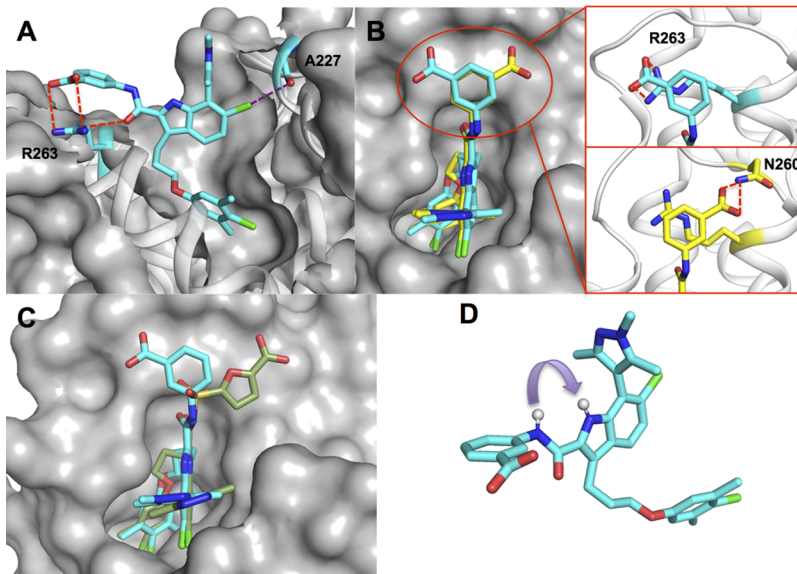
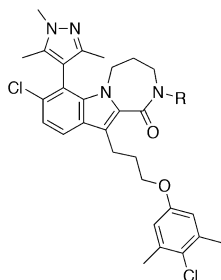


**Figure 2.** Structural data on lead compounds aided compound design. Mcl-1 residues R263, A227, and N260 are labeled. (A) One pose of amide 12 (cyan) bound Mcl-1 at the P2 pocket (SIEZ). (B) Superposition of the two binding conformations of compound 12 observed in the X-ray structure. (C) Superposition of the X-ray structures of acylsulfonamide 1 (olive) and amide 12 (cyan). (D) Mcl-1 bound conformation of amide 12 suggests tethering of two NHs by formation of a ring.

**Table 3. Binding Affinities of Tricyclic Indole-Diazepinones**



Comp.	R	K <sub>i</sub> (nM)		PAMPA (10 <sup>-6</sup> cm/s)
		Mcl-1	1% FBS <sup>a</sup>	
19		2.9 ± 0.10	27 ± 1.0	
20		4.9 ± 1.5	18 ± 5.5	143
21		1.1 ± 0.20	12 ± 2.0	
22		3.3 ± 0.61	3.8 ± 1.5	
23		2.1 ± 0.98	8.4 ± 2.6	307
24		<1.0	1.3 ± 0.7	
25		1.0 ± 0.5	91 ± 18	
26		1.2 ± 0.76	3.2 ± 1.4	
27		2.4 ± 0.65	31 ± 21	

<sup>a</sup>Mcl-1 K<sub>i</sub> in the presence of 1% fetal bovine serum.

different serum protein binding, demonstrating the importance of the heteroaromatic headpiece for determining the protein binding profile of the inhibitors. Compound 23 also shows excellent permeability assessed by PAMPA.

In summary, the tricyclic indole-diazepinone core construction not only preserves the Mcl-1 binding conformation for higher affinity but can also significantly enhance the pharmaceutical properties by eliminating two H-bond donors

and rotatable bonds. In addition, the tethering strategy also eliminates a secondary peptide bond that could be susceptible to proteolysis in the GI tract and reduce the oral bioavailability.

**X-ray Cocrystal Structure of Tricyclic Indole-Diazepinone 28 Bound to Mcl-1.** An X-ray structure of tricyclic indole-diazepinone 28 bound to Mcl-1 (Figure 3) was obtained to help identify structural features that caused the potency gain. Compound 28 adopts a similar pose compared to previously determined structures by maintaining all of the favorable hydrophobic and polar interactions at the P2 site as designed (Figure 3A). The newly formed ring locks up the binding conformation of the open-chain amide. The propylene chain of the diazepinone moiety also provides a steric barrier that reinforces the trimethylpyrazole moiety's ability to maintain an orthogonal pose to the indole core and, as a result, occupies a wider area within the hydrophobic P2 pocket. The *meta*-benzylic acid of 28 is positioned in a similar location as the furanoate of 1 (Figure 3B), whereas the carboxylates of both inhibitors form H-bonds to N260. Overall, the binding pose of 28 is very similar to that of acylsulfonamide 1. The overlay of 28 and 12 cocrystal structures shows a nearly superimposable conformation of the indole core units. However, the phenyl group of each compound is situated in a different location to engage distinctive interactions with the Mcl-1 protein (Figure 3C). Moreover, the structural information suggests that a bicyclic aromatic group may be better suited to fill the hydrophobic R263 shelf while capturing the important binding interactions of both phenyl groups.

**Tricyclic Indole Diazepinones Containing Bicyclic Headpieces.** To test this hypothesis, we constructed a parallel library of tricyclic indole diazepinones containing bicyclic headpieces. More than 100 heterobicyclic acids at varying attachment positions were directly coupled to the tricyclic indole core. Representative examples along with their biological activities are summarized in Table 4. Compounds (29–39) exhibited very potent Mcl-1 affinities even in the presence 1% FBS. In fact, the binding affinities of most compounds (except 31–33) were below the detection level able to be accurately

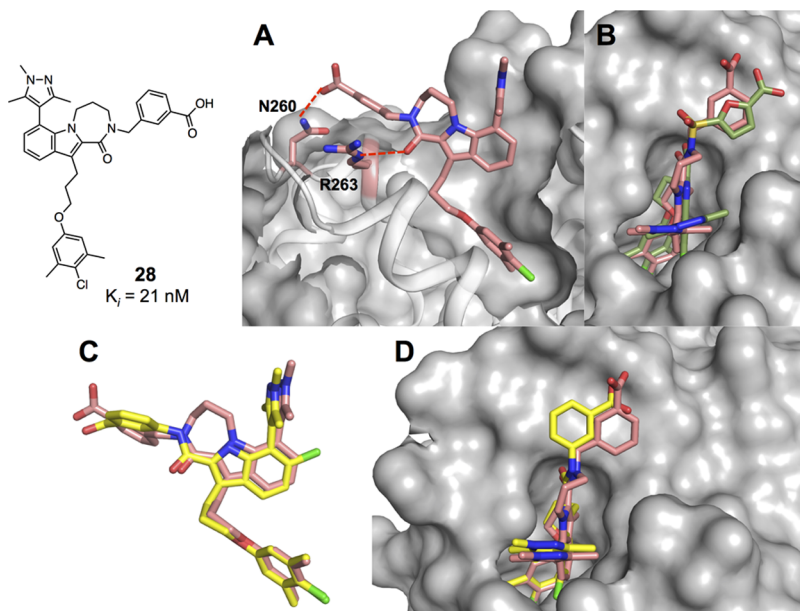


**Figure 3.** X-ray cocrystal structure of compound **28** (6BW2) aided compound design. Mcl-1 residues R263 and N260 are labeled. (A) Tricyclic indole diazepinone **28** (pink) bound Mcl-1 at the P2 pocket. (B) Superposition of the X-ray structures of acylsulfonamide **1** (olive) and compound **28** (pink). (C) Superposition of the X-ray structures of compound **28** (pink) and one pose of amide **12** (yellow) and two orientations of their overlay (C and D).

determined in our FPA assay. For accurate binding affinities to be measured for such potent compounds, a TR-FRET assay was developed using a high excess of the probe. The binding affinities measured by the TR-FRET assay were in good agreement with the data from the FPA assay and, most importantly, allowed us to rank inhibitors based on their potencies. As predicted by the structural data, both 6–5 and 6–6 fused heterocycles were found to be equally effective head groups at the R263 shelf site. Because each heterobicycle offers unique properties and SAR opportunities, it is advantageous to have multiple exchangeable pharmacophores to optimize both potency and druglike properties. Compounds **29** and **30** were found to exhibit similar Mcl-1 affinities despite the different orientations of the pyrrole portion of the indole headgroup. Three isosteric bicycles bearing different heteroatoms (**30**–**32**) could also be accommodated with a slight preference for the 4-indole-6-carboxylate of **30** over the regioisomer **31**. Interestingly, the carboxylate functional group can be introduced at multiple positions to enhance binding affinities, suggesting additional stabilizing interactions may occur between the acid and Mcl-1 residues other than N260 and R263 in the binding pocket. Of all the inhibitors synthesized, the 3-indolyl attachment in compounds **37**–**39** appears to be the preferred bicyclic headgroup arrangement with compound **39** containing the 3-indole-5-carboxylate exhibiting the highest potency ( $K_i < 100 \text{ pM}$ ). In addition, both compounds **38** and **39** exhibited subnanomolar  $K_i$ 's even in the presence of 1% FBS, which may suggest weaker serum protein binding potential due to the head groups.

**Restricted Rotation of the Trimethylpyrazole Creates Atropisomers.** The propylene chain of the diazepinone moiety forms a steric barrier to prevent the rotation of the trimethylpyrazole and creates atropisomers. These stereoisomers are noticeable in X-ray cocrystal structures where the electron density for the N-methyl group is distributed on both nitrogens of the pyrazole. In the structure, the N-methyl group of the pyrazole is positioned outside of the P2 pocket and thus

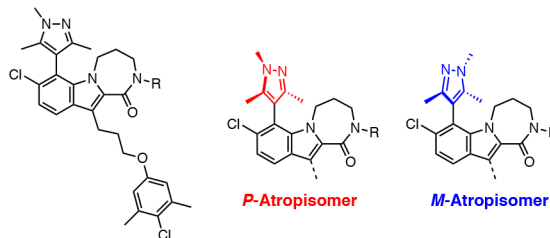
has a minimum interaction with the Mcl-1 protein; however, it is important to confirm the biological activities of separated atropisomers to validate the experimental results from the mixture. Optically pure compounds **P-39** and **M-39** were prepared and showed nearly identical Mcl-1 affinities and antiproliferative activities between stereoisomers and mixture **39**. Unless otherwise noted, all compounds are mixtures of the atropisomers, and the biological activities for the mixture are reported.

#### Selectivity Profile against Other Bcl-2 Family Proteins.

The selectivity of compounds for Mcl-1 compared to Bcl-xL and Bcl-2 was determined in the FPA assay (Table 4). All compounds tested were found to be inactive against Bcl-xL with  $K_i$ 's  $> 10 \mu\text{M}$  and exhibited minimal affinity for Bcl-2 with  $>200$ -fold window. The results indicate that all structural modifications on the series selectively enhance the Mcl-1 affinity. Therefore, as our Mcl-1 inhibitors became more potent, their selectivity was further increased. On the basis of the selectivity data, these compounds are not expected to cause thrombocytopenia mediated by excessive inhibition of Bcl-xL.

**X-ray Cocrystal Structures of Tricyclic Indole-Diazepinones **30** and **35** Bound to Mcl-1.** Two X-ray cocrystal structures of bicyclic headgroups containing tricyclic indole-diazepinones were obtained (compounds **30** and **35**), and their binding interactions with Mcl-1 were compared (Figure 4). Both compounds **30** and **35** displayed nearly identical binding conformations from the core unit to the indole headgroup (Figure 4A, B). The only difference found between these two structures was the position of the carboxylate group of each compound and their interactions with Mcl-1. The carboxylate of **30** is positioned atop the R263 to engage in a charge–charge interaction similar to one pose of amide **12** in Figure 2A and B, whereas the carboxylate in **35** makes a polar contact to the N260 side-chain NH resembling acylsulfonamide **1** (Figure 1) and compound **28** (Figure 3). These structures strongly support our design strategy of using bicyclic groups to occupy the R263 shelf for wider hydrophobic coverage and to utilize

Table 4. Biological Activities of Tricyclic Indole-Diazerpinones Containing a Bicyclic Headpiece



Comp.	R	K <sub>i</sub> (nM) FPA		K <sub>i</sub> (nM) TR-FRET		GI <sub>50</sub> (μM)		Caspase3/7 EC <sub>50</sub> (μM) H929	K <sub>i</sub> (μM) FPA		PAMPA (10 <sup>-6</sup> cm/s)
		Mcl-1	1% FBS	Mcl-1	1% FBS	H929	K562		Bcl-xL	Bcl-2	
29		<1.0	2.3 ± 1.0	0.70 ± 0.10	2.8 ± 0.75	1.4 ± 0.30	11.5 ± 1.3	0.75	19 ± 3.5	0.58 ± 0.21	21
30		<1.0	2.8 ± 1.7	0.50 ± 0.10	3.5 ± 1.0	2.0 ± 0.3	11.5 ± 1.5	0.76	>36	0.95 ± 0.33	13
31		1.8 ± 1.7	8.8 ± 4.2	3.4 ± 1.5	6.4 ± 1.2	6.1 ± 0.10	>12.5	3.5	>36	0.52 ± 0.09	
32		1.0 ± 0.20	5.8 ± 0.50	0.77 ± 0.19	3.3 ± 0.78	2.3 ± 0.10	>12.5	0.8	>36	0.55 ± 0.22	63
33		2.4 ± 1.1	8.0 ± 3.1	3.6 ± 0.28	11 ± 1.8	5.7 ± 0.10	>12.5	5.9	>36	0.44 ± 0.03	4.8
34		<1.0	4.4 ± 0.21	1.4 ± 0.10	5.0 ± 0.10	3.3 ± 0.10	6.2 ± 2.2	0.79	>36	0.49 ± 0.10	122
35		<1.0	5.2 ± 2.3	0.65 ± 0.10	1.6 ± 0.10	0.47 ± 0.10	>12.5	0.33	>36	0.14 ± 0.01	
36		<1.0	2.7 ± 0.95	0.31 ± 0.047	1.2 ± 0.37	1.0 ± 0.10	5.7 ± 1.0	0.65	11 ± 0.10	0.25 ± 0.07	4.4
37		<1.0	2.1 ± 1.7	0.46 ± 0.12	1.4 ± 0.18	1.0 ± 0.10	>9.2	0.88	21 ± 0.10	0.31 ± 0.06	
38		<1.0	<1.0	0.24 ± 0.035	0.63 ± 0.068	0.33 ± 0.10	5.8 ± 0.10	0.28	>36	0.53 ± 0.08	
39		<1.0	<1.0	0.089 ± 0.020	0.35 ± 0.15	0.30 ± 0.10	>12.5	0.077	26 ± 0.10	0.56 ± 0.11	
P-39				0.12 ± 0.03	0.32 ± 0.10	0.28 ± 0.10	>12.5				
M-39				0.11 ± 0.02	0.37 ± 0.15	0.33 ± 0.10	>12.5				

various polar interactions at the site by introducing a carboxylate group at appropriate positions.

**Mechanism-Based Cellular Activity.** For demonstrating mechanism-based cellular activity, the compounds in Table 4 were evaluated for their antiproliferative activity in the Mcl-1-dependent multiple myeloma (MM) cell line NCI H929. Conversely, the chronic myelogenous leukemia (CML) cell line K562 was found to be resistant to Mcl-1 inhibitors and served as a control for assessing off-target toxicity. Proliferation assays were carried out in both the sensitive and resistant cell lines using compounds 29–39 in culture media containing 10% FBS. These compounds were found to exhibit antiproliferative activities in a dose-dependent manner in the H929 line with GI<sub>50</sub>'s ranging from sub-μM to low μM. In addition, the cellular GI<sub>50</sub>'s were found to correlate with serum protein binding-compensated K<sub>i</sub>'s in our binding assay. Compounds 38 and 39

possessed the highest Mcl-1 affinities and exhibited the most potent cellular growth inhibition with GI<sub>50</sub>'s of 330 and 300 nM, respectively. Compound 39 showed good selectivity in the Mcl-1-resistant cell line K562 by achieving a GI<sub>50</sub> K562/GI<sub>50</sub> H929 ratio greater than 50-fold. Although moderate growth inhibition in K562 was observed for a few compounds, the K562 GI<sub>50</sub>'s appeared to be independent of the Mcl-1 affinities, suggesting that observed K562 activities were likely due to off-target effects.

For the mechanism-based effects on the modulation of apoptosis to be confirmed, compounds 29–39 were tested for their abilities to induce caspase activation in H929 cells. The assay was performed in culture medium containing 5% FBS to reduce plasma interference. Caspase 3/7 activities were measured after a 3 h incubation period. Rapid dose-dependent caspase 3/7 activation was observed for compounds 29–39 in

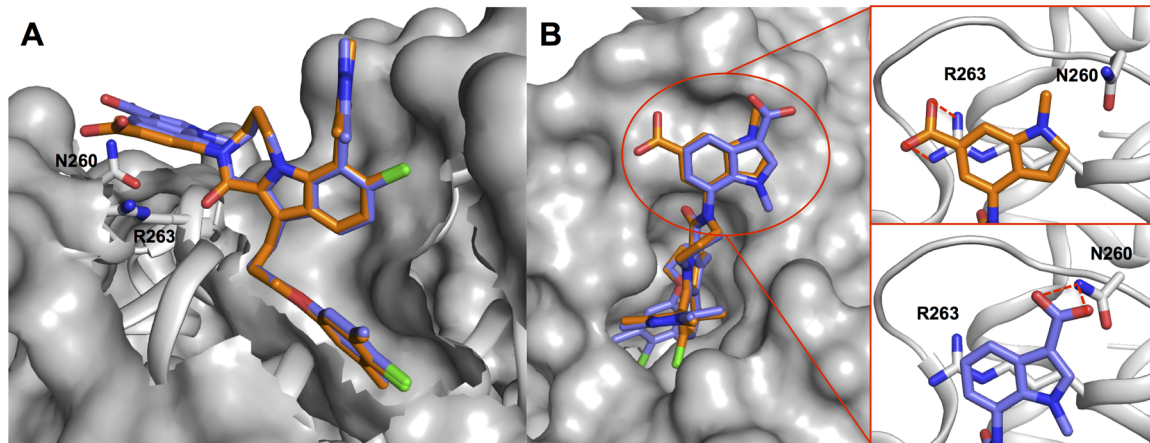


**Figure 4.** Superposition of X-ray cocrystal structures of compounds **30** (SIF4) and **35** (6BW8). Mcl-1 residues R263 and N260 are labeled. (A) Side view of Mcl-bound conformations of compounds **30** (orange) and **35** (light blue). (B) Top view of the overlaid structures.

the Mcl-1-sensitive H929 cell line as shown in Figure 5, and the EC<sub>50</sub>'s were found to correlate with the GI<sub>50</sub>'s obtained for their

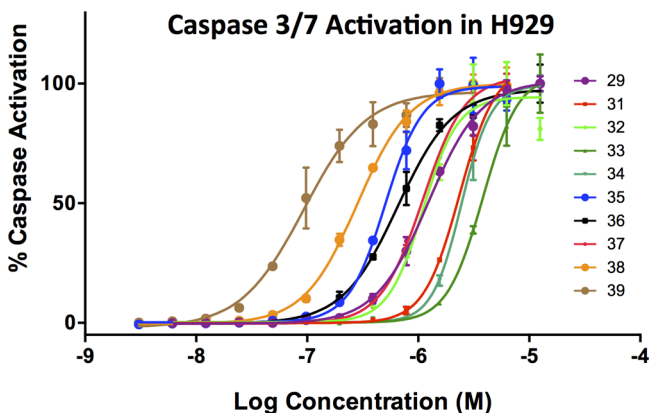
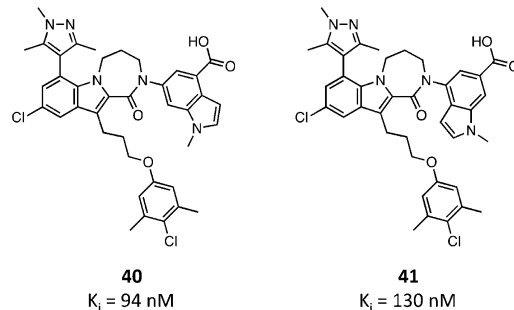


**Figure 5.** Caspase activation studies in the Mcl-1-sensitive H929 cell line by Mcl-1 inhibitors. All compounds exhibit dose-dependent activities.

antiproliferation effects. The same experiment was performed using the resistant K562 cells, but no measurable caspase activity was detected by any compounds. These results strongly suggest that the growth inhibition observed by our Mcl-1 inhibitors is mainly due to the intrinsic apoptosis mechanism that is mediated by the selective inhibition of Mcl-1 function only in the sensitive cell line.

The mechanism-based cellular activity was investigated further using the negative control chemical probes **40** and **41**. These compounds exhibit 2 orders of magnitude weaker Mcl-1 binding affinities compared to their regioisomers **29** and **30**, respectively. Because each set of isomers share identical chemical composition and functional groups, their physical properties, such as aqueous solubility, passive permeability, and serum protein binding potential, are expected to be very similar to each other despite significant differences in Mcl-1 potency. Antiproliferative activities of two sets of isomers were determined in a panel of Mcl-1-sensitive lines including MV-4-11, OPM-2, H929, ALMC-1, and ALMC-2 along with the resistant cell line K562. The results are summarized in Table 5. As expected, active isomers **29** and **30** exhibited significantly higher growth inhibition in all sensitive cells compared to that

**Table 5. Antiproliferative Activities of Active (**29** and **30**) Relative to Inactive (**40** and **41**) Regioisomers in Mcl-1-Sensitive Cell Lines**



**40**  $K_i = 94 \text{ nM}$       **41**  $K_i = 130 \text{ nM}$

comp	GI <sub>50</sub> ( $\mu\text{M}$ )					
	MV-4-11	OPM-2	H929	ALMC-1	ALMC-2	K562
<b>29</b>	0.77	1.4	1.6	1.5	3.2	11
<b>40</b>	6.2	5.7	6.0	6.6	9.9	7.7
<b>30</b>	0.95	1.7	1.7	1.7	3.3	10
<b>41</b>	9.1	8.9	10	7.7	12	10

of the resistant K562 cell line. On the other hand, the cellular effects caused by negative probes **40** and **41** are indistinguishable in all lines including K562 (Figure 6). It is intriguing that the observed cell-line dependent sensitivity profiles by active isomers **29** and **30** are nearly identical by showing the most robust growth inhibition in MV-4-11 and the weakest effects in ALMC-2. It is noteworthy that ALMC-2 was established from the same patient of ALMC-1 after symptomatic relapse with elevated Mcl-1 expression.<sup>43</sup> Negative probe **40** appears to be generally more cytotoxic than **41** in all cell lines including the resistant line. Finally, all four compounds are equally inactive in the K562 cell line, confirming the on-target mechanism-based activity in all sensitive cells.

**Synthesis.** The synthetic routes employed for the preparation of the indole core units were reported previously.<sup>39,41,42</sup> All compounds were synthesized according to methods outlined in Scheme 1. Commercially available amines or anilines were coupled to the 2-indole carboxylic acid intermediates,<sup>39,42</sup> and subsequent saponification gave the linear series indole amides **4–18**. Linear amides were cyclized using 1,3-dibromopropane under basic conditions to prepare the initial tricyclic indole diazepinone compounds **19–27**. For

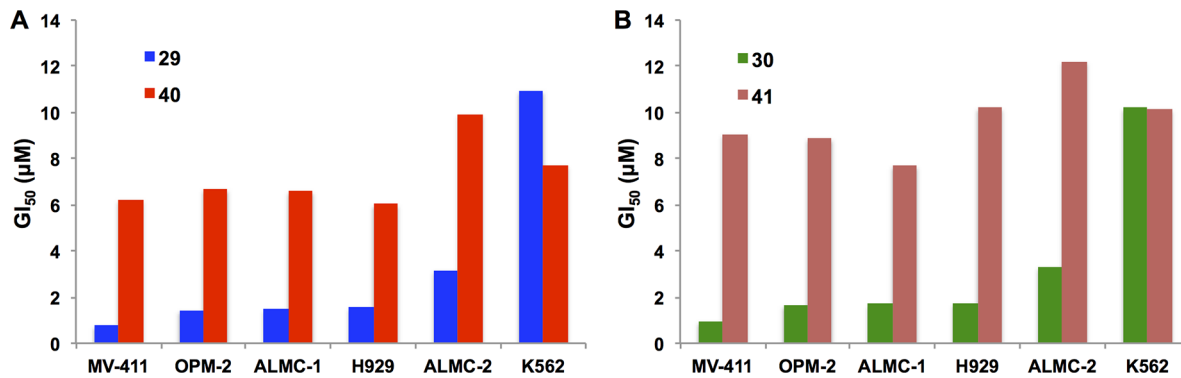
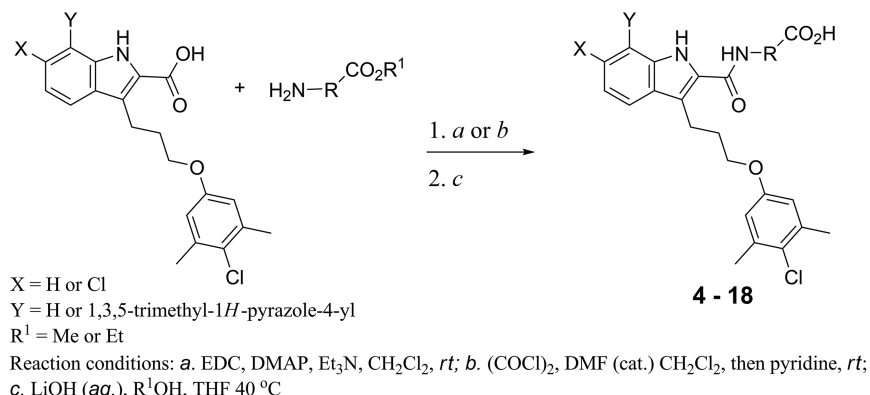


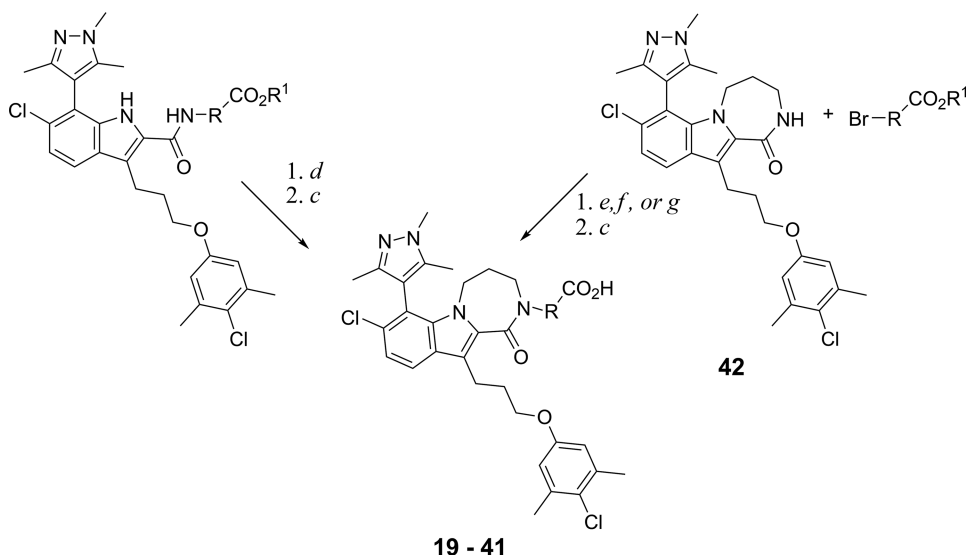
Figure 6. Growth inhibition comparison between active vs inactive regioisomers: (A) 29 (active) vs 40 (inactive), (B) 30 (active) vs 41 (inactive).

**Scheme 1. Preparation of the Linear and Cyclic-Substituted Indole Amide Derivatives**

**Linear series**



**Tricyclic series**



Reaction conditions: d. 1,3-dibromopropane,  $\text{Cs}_2\text{CO}_3$ , DMF, 80 °C; e. NaH, DMF, TBAI, rt; f.  $\text{Pd}_2(\text{dba})_3$ , Xantphos,  $\text{Cs}_2\text{CO}_3$ , dioxane, 110 °C; g. ( $\pm$ )-trans- $N^1,N^2$ -dimethylcyclohexane-1,2-diamine, CuI,  $\text{K}_2\text{CO}_3$ , toluene, 110 °C

the second series of tricycles containing bicyclic acid head groups, commercially available heterobicyclic esters were coupled to tricyclic indole lactam intermediate 42 using either the Buchwald coupling reaction or the Ullman coupling

protocol in a parallel format.<sup>42</sup> All coupled products were then saponified to give the final carboxylic acids 29–39. Experimental details are described in the Supporting Information.

**Preparation of Separated Atropisomers of 39.** The racemic 8-chloro-11-(3-(4-chloro-3,5-dimethylphenoxy)-propyl)-7-(1,3,5-trimethyl-1*H*-pyrazol-4-yl)-2,3,4,5-tetrahydro-1*H*-[1,4]diazepino[1,2-*a*]indol-1-one was separated by normal phase chiral HPLC to give optically pure *p*- and *m*-stereoisomers. The absolute configuration of the *p*-isomer (**P-42**) was determined by single crystal X-ray diffraction, and the 3D structure is shown in Figure 7. Optically pure compounds **P-39** and **M-39** were prepared using the corresponding resolved tricyclic indole cores, separately.

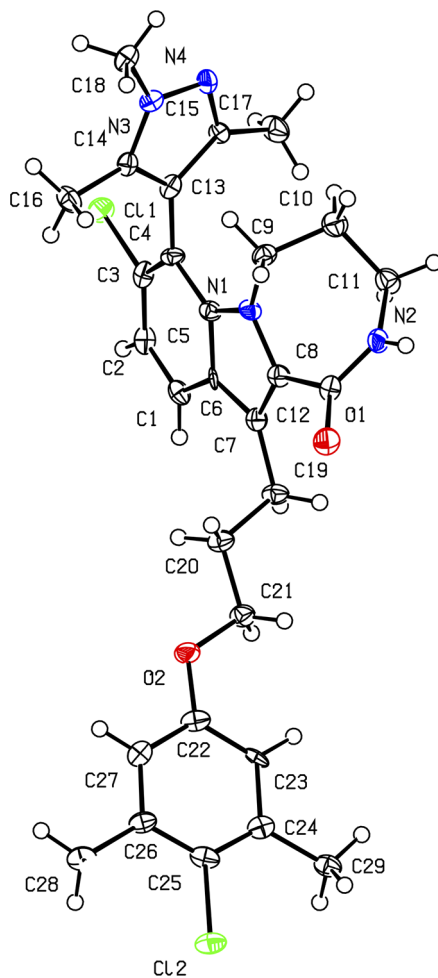


Figure 7. Single-crystal X-ray structure of the separated tricyclic indole diazepinone **P-42**.

## CONCLUSIONS

We describe a series of Mcl-1 inhibitors containing a tricyclic indole diazepinone core scaffold that were optimized using structure-based design. In this series, the acylsulfonamide functionality of 2-indole-acylsulfonamide lead compound was replaced with an amide group at the indole ring for enhancing the pharmaceutical properties. The reduced potency caused by eliminating the charge–charge interaction at the P2 pocket was regained by the introduction of a carboxylate group on a suitable aromatic headgroup to elicit new electrostatic contacts in the R263 shelf region. Structure-guided cyclization of the linear indole amide to the tricyclic indole diazepinone permanently fixed the bound conformation and significantly enhanced the binding affinity to Mcl-1. This chemical

transformation also removed two H-bond donors and rotatable bonds, which resulted in an improvement in passive permeability as assessed by PAMPA. In addition, expansion of the monocyclic headgroup to a fused bicycle further increased the binding affinity and resulted in the discovery of picomolar Mcl-1 inhibitors. These compounds exhibited robust and selective antiproliferative activities only in Mcl-1-sensitive cell lines in a dose-dependent manner. The mechanism of action was confirmed using a caspase induction assay in the same cell lines. A dose-dependent increase in caspase3/7 activity was observed, and the measured EC<sub>50</sub>'s were in good agreement with the GI<sub>50</sub>'s observed for their antiproliferative activities. In addition, the regioisomeric negative probes **40** and **41**, which bind to Mcl-1 with 2 orders of magnitude weaker affinity compared to their active analogues **29** and **30**, exhibited minimum cellular activities in both the Mcl-1-sensitive and insensitive cell lines H929 and K562, respectively. These results strongly suggest that the observed antiproliferative activities by these potent inhibitors are mediated by the caspase activation induced by the inhibition of Mcl-1. Current efforts are focused on further optimization of the potency, pharmaceutical, and pharmacokinetic properties of this series to obtain Mcl-1 inhibitors that are suitable for clinical development. Although other Mcl-1 inhibitors are already in the clinic, these compounds represent very different chemical structures, physical properties, and pharmacological profiles. It would be important to have a new class of potent Mcl-1 inhibitors to overcome the possible structure-related limitations of the previously described compounds in the clinic.

## EXPERIMENTAL SECTION

**Chemistry. General.** All NMR spectra were recorded at room temperature on a 400 MHz AMX Bruker spectrometer. <sup>1</sup>H chemical shifts are reported in  $\delta$  values in ppm downfield with the deuterated solvent as the internal standard. Data are reported as follows: chemical shift, multiplicity (s = singlet, d = doublet, t = triplet, q = quartet, br = broad, m = multiplet), integration, coupling constant (Hz). Low-resolution mass spectra were obtained on an Agilent 1200 series 6140 mass spectrometer with electrospray ionization. All samples were of  $\geq 95\%$  purity as analyzed by LC-UV/vis-MS. Analytical HPLC was performed on an Agilent 1200 series with UV detection at 214 and 254 nm along with ELS detection. LC/MS parameters were as follows: Phenomenex-C18 Kinetex column, 50  $\times$  2.1 mm, 2 min gradient, 5% (0.1% TFA/MeCN)/95% (0.1% TFA/H<sub>2</sub>O) to 100% (0.1% TFA/MeCN). Preparative purification was performed on a Gilson HPLC (Phenomenex-C18, 100  $\times$  30 mm, 10 min gradient, 5  $\rightarrow$  95% MeCN/H<sub>2</sub>O with 0.1% TFA) or by automated flash column chromatography (Isco, Inc. 100sg CombiFlash). Solvents for extraction, washing, and chromatography were HPLC grade. All reagents were purchased from chemical suppliers and used without purification.

**Protein Expression and Purification.** The Mcl-1 (172–327) protein was expressed in *Escherichia coli* BL21 CodonPlus (DE3) RIL (Stratagene). The details of design, characterization, and sequence of this construct have been described previously.<sup>39–42</sup> The protein was further purified through affinity column and size-exclusion column at 4 °C.

**Protein Crystallization, Data Collection, and Structure Refinement.** Structural studies were performed as previously described.<sup>39–42</sup> A solution of Mcl-1 protein with a small-molecule ligand (1.2× excess) was screened for crystallization conditions using commercial kits. The crystals appeared within a few weeks at room temperature or 4 °C. The single crystals were picked and frozen in liquid nitrogen in mother liquor containing 20% glycerol. Data were collected on the Life Sciences Collaborative Access Team (LS-CAT) 21-ID-G and 21-ID-F beamlines at the Advanced Photon Source (APS), Argonne National Laboratory. The data were indexed, integrated, and scaled with

HKL2000.<sup>44</sup> Using a previously determined Mcl-1 complex structure (PDB: 5IEZ) as a searching model, phasing was done by molecular replacement with Phaser<sup>45</sup> as implemented in CCP4.<sup>46</sup> Refinement of the structural models was performed with Phenix and included rounds of manual model building in COOT.<sup>47</sup> The complex was refined to resolution of 2.75 Å (28) and 2.91 Å (45). The final models have Rwork/Rfree 0.26/0.33 (28) and Rwork/Rfree 0.22/0.28 (45), respectively (Table S1).

**Competition Assays.** A fluorescein isothiocyanate (FITC)-labeled BH3 peptide derived from Bak (FITC-Bak-BH3; FITC-AHx-GQVG-RQLAIIGDDINR-NH<sub>2</sub>) and Bcl-2-interacting mediator of cell death (Bim) (FITC-Bim; FITC-AHx-EARIAQELRRIGDEFNETYTR-NH<sub>2</sub>) were purchased from GenScript and used without further purification. Fluorescence polarization anisotropy (FPA) measurements were carried out in 384-well, black, flat-bottom plates (Greiner Bio-One) using the BioTek Cytation 3 plate reader.

FPA assay conditions: The assay was carried out in 20 mM TRIS pH 7.5 buffer containing 50 mM NaCl, 3 mM DTT, 0.01% CHAPS, FITC-probe/protein (10 nM FITC-Bak-BH3 peptide/15 nM Mcl-1, 1 nM FITC-Bim-BH3 peptide/1.5 nM Mcl-1, 10 nM FITC-Bak-BH3 peptide/15 nM Bcl-xL or Bcl-2), and 5% final DMSO. Fetal calf serum (1%) is added to the 1% FBS assay. For IC<sub>50</sub> determination, compounds were diluted in DMSO in a 10-point, 3-fold serial dilution scheme, added to assay plates, and incubated for 1.5 h at room temperature. The change in anisotropy was measured and used to calculate an IC<sub>50</sub> (inhibitor concentration at which 50% of bound probe is displaced) by fitting the anisotropy data using XLFit (IDBS) to a four parameter dose-response (variable slope) equation. This was converted into a binding dissociation constant ( $K_i$ ) according to the formula:<sup>48</sup>  $K_i = [I]_{50}/([L]_{50}/K_d + [P]_0/K_d + 1)$ , where [I]<sub>50</sub> is the concentration of the free inhibitor at 50% inhibition, [L]<sub>50</sub> is the concentration of the free labeled ligand at 50% inhibition, [P]<sub>0</sub> is the concentration of the free protein at 0% inhibition, and K<sub>d</sub><sup>pep</sup> represents the dissociation constant of the FITC-labeled peptide probe. Compounds were evaluated using replicate measurements in duplicate; K<sub>i</sub> values shown are the average of duplicate values.

TR-FRET assay conditions: In the assay buffer described above, we added 300 nM FITC-BAK-BH3 peptide, 1 nM Mcl-1-MBP fusion, 1 nM MBP-terbium (Cisbio, Bedford, MA, USA), and 0.05% Pluronic F-68 (Sigma-Aldrich, St. Louis, MO, USA). Mixtures were incubated for 3 h, and signal (Delta F) was measured on the Biotek Cytation 3 equipped with a filter cube containing an Ex 340/30 nm Em 620/10 filter and an Ex 340/30 nm Em 520 filter.

K<sub>i</sub> values were calculated as described above.

**Cell Line Proliferation Assay.** Cells were dispensed into 96-well plates at a concentration of 3000 cells per well in RPMI supplemented with 10% FBS and 0.05 mM 2-mercaptoethanol and incubated overnight at 37 °C in a tissue culture incubator. Compounds were diluted in DMSO (0.5%) and added to the wells. Plates were incubated for 72 h, and cell viability was measured using the Cell TiterGlo reagent. %Viability was defined as relative luminescence units (RLU) of each well divided by the RLU of cells on day 0. Dose-response curves were generated, and GI<sub>50</sub> values were determined using XLFIT (IDBS, Guildford, UK) software.

**Caspase Activation Assay.** Cells (5000 cells/well) were dispensed in 96-well plates as described in the proliferation assay methods with 5% FBS. Plates were incubated with compounds for 3 h; 100 μL of Caspase-Glo (Promega, Madison, WI, USA) reagent was added, and the mixture was incubated at room temperature in the dark for 30 min. Luminescence was measured (Biotek Cytation 3) and analyzed using XLFIT (IDBS) to generate EC<sub>50</sub> values.

**Absolute Configuration Determination of Compound P-42.** A supersaturated solution of the resolved isomer (peak 2) in a hexane/ethyl acetate mixture at 60 °C was crystallized by slowly cooling to room temperature. Data were collected on a Bruker X8Proteum goniometer equipped with a Proteum PT<sub>135</sub> CCD detector. The crystal diffracted to 0.84 Å with 80% completeness. The data were processed using SHELXL software.<sup>49</sup> The structure was solved in a monoclinic P2<sub>1</sub> space group with the unit cell dimensions of a = 12.9440 Å, b = 6.9840 Å, c = 15.108 Å, and α = 90.000°, β = 104.920°,

γ = 90.000°.<sup>50</sup> The final R-value is 5.1%. ORTEP images were generated in Platon.<sup>51</sup>

## ASSOCIATED CONTENT

### S Supporting Information

The Supporting Information is available free of charge on the ACS Publications website at DOI: 10.1021/acs.jmedchem.7b01155.

X-ray crystallography statistics (CSV)

Synthesis details (PDF)

### Accession Codes

Atom coordinates and structure factors for Mcl-1/ligand complexes have been deposited at the Protein Data Bank ID codes: 6BW2, 6BW8.

## AUTHOR INFORMATION

### Corresponding Author

\*Phone: +1 (615) 322 6303. Fax: +1 (615) 875 3236. E-mail: stephen.fesik@vanderbilt.edu.

### ORCID

Stephen W. Fesik: 0000-0001-5957-6192

### Present Addresses

<sup>‡</sup>S.S.: Broad Institute, Cambridge, MA

<sup>§</sup>Z.B.: AbbVie Pharmaceuticals, North Chicago, IL

<sup>†</sup>O.W.S.: The Institute of Cancer Research, Sutton, UK

### Author Contributions

<sup>†</sup>S.S. and Z. B. contributed equally to this work.

### Notes

The authors declare no competing financial interest.

## ACKNOWLEDGMENTS

The authors thank co-workers at the High-Throughput Screening Core facility of Vanderbilt University, TN, for compound management and providing the instrumentation to perform the binding assay, NCATS Chemical Genomics Center (NCGC) for providing PAMPA data, and Ms. Carrie F. Browning for contributions in the caspase3/7 activation assay development. This research was supported by the U.S. National Institutes of Health, NIH Director's Pioneer Award DP1OD006933/DP1CA174419 to S.W.F., NCI Experimental Therapeutics (NExT) Program BOA29XS129TO22 under the Leidos Biomed Prime Contract No. HHSN261200800001E, and a career development award to S.W.F. from an NCI SPORE grant in breast cancer (Grant P50CA098131) to C. L. Arteaga. The Biomolecular NMR Facility at Vanderbilt University is supported in part by NIH SIG Grant 1S-10RR025677-01 and Vanderbilt University matching funds. Use of the Advanced Photon Source was supported by the U.S. Department of Energy, Office of Science, Office of Basic Energy Sciences, under Contract No. DE-AC02-06CH11357.

## ABBREVIATIONS USED

Mcl-1, myeloid cell leukemia 1; Bcl-2, B-cell lymphoma 2; Bcl-xL, B-cell lymphoma extra large; BH3, Bcl-2 homology domain 3; Bax, Bcl-2-associated X protein; Bak, Bcl-2 homologous antagonist killer; FBS, fetal bovine serum; TR-FRET, time-resolved fluorescence energy transfer; FITC, fluorescein isothiocyanate; FPA, fluorescence polarization anisotropy

## ■ REFERENCES

- (1) Adams, J. M.; Cory, S. The Bcl-2 Apoptotic Switch in Cancer Development and Therapy. *Oncogene* **2007**, *26*, 1324–1337.
- (2) Danial, N. N.; Korsmeyer, S. J. Cell Death: Critical Control Points. *Cell* **2004**, *116*, 205–219. Ghobrial, I. M.; Witzig, T. E.; Adjei, A. A. Targeting Apoptosis Pathways in Cancer Therapy. *Cancer J. Clin.* **2005**, *55*, 178–194.
- (3) Reed, J. C. Bcl-2 And The Regulation of Programmed Cell Death. *J. Cell Biol.* **1994**, *124*, 1–6. Kitanaka, C.; Namiki, T.; Noguchi, K.; Mochizuki, T.; Kagaya, S.; Chi, S.; Hayashi, A.; Asai, A.; Tsujimoto, Y.; Kuchino, Y. Caspase-Dependent Apoptosis of COS-7 Cells Induced by Bax Overexpression: Differential Effects of Bcl-2 and Bcl-XL on Bax-Induced Caspase Activation and Apoptosis. *Oncogene* **1997**, *15*, 1763–1772.
- (4) Vogler, M.; Dinsdale, D.; Dyer, M. J.; Cohen, G. M. Bcl-2 Inhibitors: Small Molecules with a Big Impact on Cancer Therapy. *Cell Death Differ.* **2009**, *16*, 360–367.
- (5) Czabotar, P. E.; Lessene, G.; Strasser, A.; Adams, J. M. Control of Apoptosis by The BCL-2 Protein Family: Implications for Physiology and Therapy. *Nat. Rev. Mol. Cell Biol.* **2014**, *15*, 49–63.
- (6) Hanahan, D.; Weinberg, R. A. The Hallmarks of Cancer. *Cell* **2000**, *100*, 57–70.
- (7) Placzek, W. J.; Wei, J.; Kitada, S.; Zhai, D.; Reed, J. C.; Pellecchia, M. A. A Survey of The Anti-Apoptotic Bcl-2 Subfamily Expression in Cancer Types Provides a Platform to Predict the Efficacy of Bcl-2 Antagonists in Cancer Therapy. *Cell Death Dis.* **2010**, *1*, e40.
- (8) Beroukhim, R.; Mermel, C. H.; Porter, D.; Wei, G.; Raychaudhuri, S.; Donovan, J.; Barrette, J.; Boehm, J. S.; Dobson, J.; Urashima, M.; McHenry, K. T.; Pinchback, R. M.; Ligon, A. H.; Cho, Y. J.; Haery, L.; Greulich, H.; Reich, M.; Winckler, W.; Lawrence, M. S.; Weir, B. A.; Tanaka, K. E.; Chiang, D. Y.; Bass, A. J.; Loo, A.; Hoffman, C.; Presner, J.; Liefeld, T.; Gao, Q.; Yecis, D.; Signoretti, S.; Maher, E.; Kaye, F. J.; Sadaki, H.; Tepper, J. E.; Fletcher, J. A.; Tabernero, J.; Baselga, J.; Tsao, M. S.; Demichelis, F.; Rubin, M. A.; Janne, P. A.; Daly, M. J.; Nucera, C.; Levine, R. L.; Ebert, B. L.; Gabriel, S.; Rustgi, A. K.; Antonescu, C. R.; Ladanyi, M.; Letai, A.; Garraway, L. A.; Loda, M.; Beer, D. G.; True, L. D.; Okamoto, A.; Pomeroy, S. L.; Singer, S.; Golub, T. R.; Lander, E. S.; Getz, G.; Sellers, W. R.; Meyerson, M. The Landscape of Somatic Copy-Number Alteration Across Human Cancers. *Nature* **2010**, *463*, 899–905.
- (9) Wei, G.; Margolin, A. A.; Haery, L.; Brown, E.; Cucolo, L.; Julian, B.; Shehata, S.; Kung, A. L.; Beroukhim, R.; Golub, T. R. Chemical Genomics Identifies Small-Molecule MCL1 Repressors and BCL-XL as a Predictor of MCL1 Dependency. *Cancer Cell* **2012**, *21*, 547–562.
- (10) Song, L.; Coppola, D.; Livingston, S.; Cress, D.; Haura, E. B. Mcl-1 Regulates Survival and Sensitivity to Diverse Apoptotic Stimuli in Human Non-Small Cell Lung Cancer Cells. *Cancer Biol. Ther.* **2005**, *4*, 267–276.
- (11) Ding, Q.; He, X.; Xia, W.; Hsu, J.-M.; Chen, C.-T.; Li, L.-Y.; Lee, D.-F.; Yang, J.-Y.; Xie, X.; Liu, J.-C.; Hung, M.-C. Myeloid Cell Leukemia-1 Inversely Correlates With Glycogen Synthase Kinase-3beta Activity And Associates With Poor Prognosis In Human Breast Cancer. *Cancer Res.* **2007**, *67*, 4564–4571.
- (12) Krajewska, M.; Krajewski, S.; Epstein, J. I.; Shabaik, A.; Sauvageot, J.; Song, K.; Kitada, S.; Reed, J. C. Immunohistochemical Analysis of Bcl-2, Bax, Bcl-x, And Mcl-1 Expression in Prostate Cancers. *Am. J. Pathol.* **1996**, *148*, 1567–1576.
- (13) Miyamoto, Y.; Hosotani, R.; Wada, M.; Lee, J. U.; Koshiba, T.; Fujimoto, K.; Tsuji, S.; Nakajima, S.; Doi, R.; Kato, M.; Shimada, Y.; Imamura, M. Immunohistochemical Analysis of Bcl-2, Bax, Bcl-X, and Mcl-1 Expression in Pancreatic Cancers. *Oncology* **1999**, *56*, 73–82.
- (14) Brotin, E.; Meryet-Figuierre, M.; Simonin, K.; Duval, R. E.; Villedieu, M.; Leroy-Dudal, J.; Saison-Behmoaras, E.; Gauduchon, P.; Denoyelle, C.; Poulain, L. Bcl-XL and MCL-1 Constitute Pertinent Targets in Ovarian Carcinoma and Their Concomitant Inhibition Is Sufficient to Induce Apoptosis. *Int. J. Cancer* **2010**, *126*, 885–895.
- (15) Derenne, S.; Monia, B.; Dean, N. M.; Taylor, J. K.; Rapp, M. J.; Harousseau, J.-L.; Bataille, R.; Amiot, M. Antisense Strategy Shows That Mcl-1 Rather Than Bcl-2 Or Bcl-xL Is An Essential Survival Protein of Human Myeloma Cells. *Blood* **2002**, *100*, 194–199.
- (16) Andersen, M. H.; Becker, J. C.; Thor Straten, P. The Antiapoptotic Member of The Bcl-2 Family Mcl-1 Is a CTL Target In Cancer Patients. *Leukemia* **2005**, *19*, 484–485.
- (17) Kang, M. H.; Wan, Z.; Kang, Y. H.; Spoto, R.; Reynolds, C. P. Mechanism Of Synergy Of N-(4-Hydroxyphenyl)Retinamide and ABT-737 in Acute Lymphoblastic Leukemia Cell Lines: Mcl-1 Inactivation. *J. Natl. Cancer Inst.* **2008**, *100*, 580–595.
- (18) Wertz, I. E.; Kusam, S.; Lam, C.; Okamoto, T.; Sandoval, W.; Anderson, D. J.; Helgason, E.; Ernst, J. A.; Eby, M.; Liu, J.; Belmont, L. D.; Kaminker, J. S.; O'Rourke, K. M.; Pujara, K.; Kohli, P. B.; Johnson, A. R.; Chiu, M. L.; Lill, J. R.; Jackson, P. K.; Fairbrother, W. J.; Seshagiri, S.; Ludlam, M. J.; Leong, K. G.; Dueber, E. C.; Maecker, H.; Huang, D. C.; Dixit, V. M. Sensitivity To Antitubulin Chemotherapeutics Is Regulated by Mcl-1 And FBW7. *Nature* **2011**, *471*, 110–114.
- (19) Wei, S. H.; Dong, K.; Lin, F.; Wang, X.; Li, B.; Shen, J. J.; Zhang, Q.; Wang, R.; Zhang, H. Z. Inducing Apoptosis and Enhancing chemosensitivity to Gemcitabine Via RNA Interference Targeting Mcl-1 Gene in Pancreatic Carcinoma Cell. *Cancer Chemother. Pharmacol.* **2008**, *62*, 1055–1064.
- (20) Delbridge, A. R.; Strasser, A. The BCL-2 Protein Family, BH3-Mimetics and Cancer Therapy. *Cell Death Differ.* **2015**, *22*, 1071–1080.
- (21) Arkin, M. R.; Wells, J. A. Small-Molecule Inhibitors of Protein-Protein Interactions: Progressing Towards the Dream. *Nat. Rev. Drug Discovery* **2004**, *3*, 301–317.
- (22) Petros, A. M.; Olejniczak, E. T.; Fesik, S. W. Structural Biology Of The Bcl-2 Family Of Proteins. *Biochim. Biophys. Acta, Mol. Cell Res.* **2004**, *1644*, 83–94.
- (23) Stewart, M. L.; Fire, E.; Keating, A. E.; Walensky, L. D. The MCL-1 BH3 Helix Is an Exclusive MCL-1 Inhibitor and Apoptosis Sensitizer. *Nat. Chem. Biol.* **2010**, *6*, 595–601.
- (24) Czabotar, P. E.; Lee, E. F.; van Delft, M. F.; Day, C. L.; Smith, B. J.; Huang, D. C.; Fairlie, W. D.; Hinds, M. G.; Colman, P. M. Structural Insights into the Degradation of Mcl-1 Induced by BH3 Domains. *Proc. Natl. Acad. Sci. U. S. A.* **2007**, *104*, 6217–6222.
- (25) Kaefer, A.; Yang, J.; Noertersheuser, P.; Mensing, S.; Humerickhouse, R.; Awani, W.; Xiong, H. Mechanism-Based Pharmacokinetic/Pharmacodynamic Meta-Analysis of Navitoclax (ABT-263) Induced Thrombocytopenia. *Cancer Chemother. Pharmacol.* **2014**, *74*, 593–602.
- (26) Souers, A. J.; Leverton, J. D.; Boghaert, E. R.; Ackler, S. L.; Catron, N. D.; Chen, J.; Dayton, B. D.; Ding, H.; Enschede, S. H.; Fairborther, W. J.; Huang, D. C.; Hymowitz, S. G.; Jin, S.; Khaw, S. L.; Kovar, P. J.; Lam, L. T.; Lee, J.; Maecker, H. L.; Marsh, K. C.; Mason, K. D.; Mitten, M. J.; Nimmer, P. M.; Oleksijew, A.; Park, C. H.; Park, C. M.; Phillips, D. C.; Roberts, A. W.; Sampath, D.; Seymour, J. F.; Smith, M. L.; Sullivan, G. M.; Tahir, S. K.; Tse, C.; Wendt, M. D.; Xiao, Y.; Xue, J. C.; Zhang, H.; Humerickhouse, R. A.; Rosenberg, S. H.; Elmore, S. W. ABT-199, a Potent and Selective BCL-2 Inhibitor, Achieves Antitumor Activity While Sparing Platelets. *Nat. Med.* **2013**, *19*, 202–208.
- (27) U.S. FDA News release. April 11, 2016.
- (28) Tse, C.; Shoemaker, A. R.; Adickes, J.; Anderson, M. G.; Chen, J.; Jin, S.; Johnson, E. F.; Marsh, K. C.; Mitten, M. J.; Nimmer, P.; Roberts, L.; Tahir, S. K.; Xiao, Y.; Yang, X.; Zhang, H.; Fesik, S.; Rosenberg, S. H.; Elmore, S. W. ABT-263: a Potent and Orally Bioavailable Bcl-2 Family Inhibitor. *Cancer Res.* **2008**, *68*, 3421–3428.
- (29) Gandhi, L.; Camidge, D. R.; de Oliveira, M. R.; Bonomi, P. D.; Gandara, D.; Khaira, D.; Hann, C. L.; McKeegan, E. M.; Litvinovich, E.; Hemken, P. M.; Dive, C.; Enschede, S. H.; Nolan, C.; Chiu, Y.; Busman, T.; Xiong, H.; Krivoshik, A. P.; Humerickhouse, R.; Shapiro, G. I.; Rudin, C. M. Phase I Study of Navitoclax (ABT-263), a Novel Bcl-2 Family Inhibitor, in Patients With Small-Cell Lung Cancer and Other Solid Tumors. *J. Clin. Oncol.* **2011**, *29*, 909–916.
- (30) Rudin, C. M.; Hann, C. L.; Garon, E. B.; de Oliveira, M. R.; Bonomi, P. D.; Camidge, D. R.; Chu, Q.; Giaccone, G.; Khaira, D.;

- Ramalingam, S. S.; Ranson, M. R.; Dive, C.; McKeegan, E. M.; Chyla, B. J.; Dowell, B. L.; Chakravarthy, A.; Nolan, C. E.; Rudersdorf, N.; Busman, T. A.; Mabry, M. H.; Krivoshik, A. P.; Humerickhouse, R. A.; Shapiro, G. I.; Gandhi, L. Phase II Study of Single-Agent Navitoclax (ABT-263) and Biomarker Correlates in Patients with Relapsed Small Cell Lung Cancer. *Clin. Cancer Res.* **2012**, *18*, 3163–3169.
- (31) Wendt, M. D. The Discovery of Navitoclax, a Bcl-2 Family Inhibitor. *Top. Med. Chem.* **8** (*Protein-Protein Interactions*); Springer-Verlag: Berlin Heidelberg, 2012, 231–258.
- (32) Kotschy, A.; Szlavik, Z.; Murray, J.; Davidson, J.; Maragno, A. L.; Le Toumelin-Braizat, G.; Chanrion, M.; Kelly, G. L.; Gong, J.; Moujalled, D. M.; Bruno, A.; Csekei, M.; Paczal, A.; Szable, Z. B.; Sipos, S.; Radics, G.; Proszenyak, A.; Balint, B.; Ondi, L.; Blasko, G.; Robertson, A.; Surgenor, A.; Dokurno, P.; Chen, I.; Matassova, N.; Smith, J.; Pedder, C.; Graham, C.; Studeny, A.; Lysiak-Auvity, G.; Girard, A.; Gravé, F.; Segal, D.; Riffkin, C. D.; Pomilio, G.; Galbraith, L. C. A.; Aubrey, B. J.; Brennan, M. S.; Herold, M. J.; Chang, C.; Guasconi, G.; Cauquil, N.; Melchiore, F.; Guigal-Stephan, N.; Lockhart, B.; Colland, F.; Hickman, J. A.; Roberts, A. W.; Huang, D. C. S.; Wei, A. H.; Strasser, A.; Lessene, G.; Geneste, O. The MCL1 Inhibitor S63845 Is Tolerable and Effective in Diverse Cancer Models. *Nature* **2016**, *538*, 477–482.
- (33) Kotschy, A.; Szlavik, Z.; Csekel, M.; Paczal, A.; Szabo, Z.; Sipos, S.; Radics, G.; Proszenyak, A.; Balint, B.; Bruno, A.; Geneste, O.; Davidson, J. E. P.; Murray, J. B.; Chen, I.; Perron-Sierra, F. New Thienopyrimidine Derivatives, a Process for Their Preparation and Pharmaceutical Compositions Containing Them. *Eur. Pat. Appl.* 2015, EP 2886545A1 20150624.
- (34) Szlavik, Zoltan; Balint, B.; Kotschy, A.; Chanrion, M.; Geneste, O.; Davidson, J. E.P.; Murray, J. B.; Sipos, S.; Proszenyak, A. New Hydroxyacid Derivatives, a Process for Their Preparation and Pharmaceutical Compositions Containing Them. *PCT Int. Appl.* 2016 WO2016207216A1.
- (35) Szlavik, Z.; Kotschy, A.; Chanrion, M.; Marles, D.; Geneste, O.; Davidson, J. E.P.; Murray, J. B.; Sipos, S.; Paczal, A.; Balint, B. New Hydroxyester Derivatives, a Process for Their Preparation and Pharmaceutical Compositions Containing Them. *PCT Int. Appl.* 2016, WO2016207225A1.
- (36) Szlavik, Z.; Szabo, Z.; Csekel, M.; Paczal, A.; Kotschy, A.; Bruno, A.; Geneste, O.; Chen, I.; Davidson, J. E. P.; Murray, J. B.; Ondi, L.; Radics, G.; Sipos, S.; Proszenyak, A.; Perron-Sierra, F.; Balint, B. New Aminoacid Derivatives, a Process for Their Preparation and Pharmaceutical Compositions Containing Them. *PCT Int. Appl.* 2016, WO2016207226A1.
- (37) Brown, S. P.; Li, Y.; Lizarzaburu, M. E.; Lucas, B. S.; Paras, N. A.; Taygerly, J.; Vimolratana, M.; Wang, X.; Yu, M.; Zancanella, M.; Zhu, L.; Gonzales Buenrostro, A.; Li, Z. Tetrahydronaphthalene Derivatives that Inhibit Mcl-1 Protein. *PCT Int. Appl.* 2016, WO2016033486.
- (38) Johannes, J. W.; Bates, S.; Beigie, C.; Belmonte, M. A.; Breen, J.; Cao, S.; Centrella, P. A.; Clark, M. A.; Cuozzo, J. W.; Dumelin, C. E.; Ferguson, A. D.; Habeshian, S.; Hargreaves, D.; Joubran, C.; Kazmirski, S.; Keefe, A. D.; Lamb, M. L.; Lan, H.; Li, Y.; Ma, H.; Mlynarski, S.; Packer, M. J.; Rawlins, P. B.; Robbins, D. W.; Shen, H.; Sigel, E. A.; Soutter, H. H.; Su, N.; Troast, D. M.; Wang, H.; Wickson, K. F.; Wu, C.; Zhang, Y.; Zhao, Q.; Zheng, X.; Hird, A. W. Structure Based Design of Non-Natural Peptidic Macroyclic Mcl-1 Inhibitors. *ACS Med. Chem. Lett.* **2017**, *8*, 239–244.
- (39) Friberg, A.; Vigil, D.; Zhao, B.; Daniels, R. N.; Burke, J. P.; Garcia-Barrantes, P. M.; Camper, D.; Chauder, B. A.; Lee, T.; Olejniczak, E. T.; Fesik, S. W. Discovery of Potent Myeloid Cell Leukemia 1 (Mcl-1) Inhibitors Using Fragment-Based Methods and Structure-Based Design. *J. Med. Chem.* **2013**, *56*, 15–30.
- (40) Burke, J. P.; Bian, Z.; Shaw, S.; Zhao, B.; Goodwin, C. M.; Belmar, J.; Browning, C. F.; Vigil, D.; Friberg, A.; Camper, D. V.; Rossanese, O. W.; Lee, T.; Olejniczak, E. T.; Fesik, S. W. Discovery Of Tricyclic Indoles That Potently Inhibit Mcl-1 Using Fragment-Based Methods and Structure-Based Design. *J. Med. Chem.* **2015**, *58*, 3794–3805.
- (41) Pelz, N. F.; Bian, Z.; Zhao, B.; Shaw, S.; Tarr, J. C.; Belmar, J.; Gregg, C.; Camper, D. V.; Goodwin, C. M.; Arnold, A. L.; Sensintaffar, J. L.; Friberg, A.; Rossanese, O. W.; Lee, T.; Olejniczak, E. T.; Fesik, S. W. Discovery of 2-Indole-acylsulfonamide Myeloid Cell Leukemia 1 (Mcl-1) Inhibitors Using Fragment-Based Methods. *J. Med. Chem.* **2016**, *59*, 2054–2066.
- (42) Lee, T.; Bian, Z.; Zhao, B.; Hogdal, L. J.; Sensintaffar, J. L.; Goodwin, C. M.; Belmar, J.; Shaw, S.; Tarr, J. C.; Veerasamy, N.; Matulis, S. M.; Koss, B.; Fischer, M. A.; Arnold, A. L.; Camper, D. V.; Browning, C. F.; Rossanese, O. W.; Budhraja, A.; Opferman, J.; Boise, L. H.; Savona, M. R.; Letai, A.; Olejniczak, E. T.; Fesik, S. W. Discovery and Biological Characterization Of Potent Myeloid Cell Leukemia-1 Inhibitors. *FEBS Lett.* **2017**, *591*, 240–251.
- (43) Arendt, B. K.; Ramirez-Alvarado, M.; Sikkink, L. A.; Keats, J. J.; Ahmann, G. J.; Dispensier, A.; Fonseca, R.; Ketterling, R. P.; Knudson, R. A.; Mulvihill, E. M.; Tschumper, R. C.; Wu, X.; Zeldenrust, S. R.; Jelinek, D. F. Biologic and Genetic Characterization of the Novel Amyloidogenic Lambda Light Chain-Secreting Human Cell Lines, ALMC-1 And ALMC-2. *Blood* **2008**, *112*, 1931–1941.
- (44) Otwinowski, Z.; Minor, W. Processing of X-ray Diffraction Data Collected in Oscillation Mode. In *Macromolecular Crystallography. Part A*; Carter, C. W., Jr., Sweet, R. M., Eds.; Academic Press: San Diego, CA, 1997; Vol. 276, pp 307–326.
- (45) McCoy, A. J.; Grosse-Kunstleve, R. W.; Adams, P. D.; Winn, M. D.; Storoni, L. C.; Read, R. J. Phaser Crystallographic Software. *J. Appl. Crystallogr.* **2007**, *40*, 658–674.
- (46) Collaborative Computational Project, N.. The CCP4 Suite: Programs For Protein Crystallography. *Acta Crystallogr., Sect. D: Biol. Crystallogr.* **1994**, *50*, 760–763.
- (47) Emsley, P.; Cowtan, K. Coot: Model-Building Tools For Molecular Graphics. *Acta Crystallogr., Sect. D: Biol. Crystallogr.* **2004**, *60*, 2126–2132.
- (48) Nikolovska-Coleska, Z.; Wang, R.; Fang, X.; Pan, H.; Tomita, Y.; Li, P.; Roller, P. P.; Krajewski, K.; Saito, N. G.; Stuckey, J. A.; Wang, S. Development and Optimization of a Binding Assay for the XIAP BIR3 Domain Using Fluorescence Polarization. *Anal. Biochem.* **2004**, *332*, 261–273.
- (49) Sheldrick, G. M. SHELXT - Integrated Space-Group and Crystal-Structure Determination. *Acta Crystallogr., Sect. A: Found. Adv.* **2015**, *C71*, 3–8.
- (50) Burla, M. C.; Caliandro, R.; Carrozzini, B.; Cascarano, G. L.; Cuocci, C.; Giacovazzo, C.; Mallamo, M.; Mazzone, A.; Polidori, G. Crystal Structure Determination and Refinement via SIR2014. *J. Appl. Crystallogr.* **2015**, *48*, 306–309.
- (51) Spek, A. L. Structure Validation in Chemical Crystallography. *Acta Crystallogr., Sect. D: Biol. Crystallogr.* **2009**, *D65*, 148–155.